JOURNAL OF MATERIALS SCIENCE 31 (1996) 4647–4654

Structure and mechanical properties of internally hydrided Mg-III_a transition metal alloys

S. MOROZUMI*
Magnesium Research Center, Chiba Institute of Technology, Narashino 275, Japan
H. SAIKAWA, T. MINEGISHI
Department of Metallurgical Engineering, Chiba Institute of Technology, Narashino 275, Japan
M. MATSUYAMA, K. WATANABE
**Hydrogen Isotope Research Center, Toyama University, Toyama 930, Japan*
M. IIJIMA, M. OHTSUKI
Mitsubishi Materials Corp., Ohtemachi, Chiyoda-ku, Tokyo 100, Japan

Magnesium alloys containing III_a transition metals, such as Sc, Y and Ho, respectively, were hydrogenated at 773 K and examined for microstructure, X-ray diffraction pattern, micro-Vickers hardness, and tensile properties at room and high temperatures. Results obtained are as follows:
1. The alloys, respectively, have been internally hydrided and have precipitated hydrides of the III_a transition metals as small flake-like particles in the matrix and at grain boundaries, as well as twin boundaries.
2. The dispersed hydride particles do not necessarily contribute to further hardening of the alloys at room temperature and up to near 673 K.
3. However, the dispersed particles are very stable and seem to improve mechanical properties of the alloys above 673 K.
4. Presumed relationships of crystallographic coincidence between the matrix and hydrides have been obtained.

1. Introduction

Internal hydriding of magnesium alloys has been studied on Mg–rare earth–Zn alloys [1] and Mg–Zr alloys [2–10]. In the Mg–rare earth–Zn alloys so far studied, however, the internal hydriding was applied to liberate zinc atoms from their compounds with rare earths by forming the rare earth hydrides, in order to restore the age-hardenability of the alloys with zinc in solid solution: while in the Mg–Zr alloys dispersed zirconium hydride particles improved the strength of the alloys. The latter instance suggests that hydride-dispersed magnesium alloys can be produced by alloying with strong hydride formers, such as rare earth metals, and then heat-treating the alloys in hydrogen atmosphere. The present paper deals with structure and mechanical properties of internally hydrided magnesium alloys containing III_a transition metals, and discusses the results from a high temperature use point of view.

2. Experimental procedures

2.1. Specimens

Alloy specimens in Table I were prepared with commercial raw materials by normal melting process using flux, followed by casting into a steel mould under a low pressure of about 4 MPa. Then they were machined into various shapes of test pieces, with which microstructure observations, X-ray diffraction analysis (XRD), micro-Vickers hardness test, and tensile tests at room and high temperatures were performed. The dimensions of the tensile test specimen are 2 mm thick and 4 mm wide, in a gauge length of 20 mm.

2.2. Hydrogenation

Hydrogenation was performed by keeping finally-machined specimens, except TMY3-2, TMY3-3 and unhydrided specimens, under about 0.1 MPa of hydrogen at 773 K for 2 h (7.2×10^3 s). By this treatment, hydrogen absorption almost ceases, that is, the specimen is fully hydrogenated. However, TMY3-2 and TMY3-3, designated as 1/2 and 1/3 hydrogenated specimens, respectively, were kept for 16 and 9 min (960 and 540 s), respectively, under the same hydrogen pressure and temperature. Unhydrided specimens were annealed at 773 K for 1 h (3.6×10^3 s), except unhydrided TMY3 which was heat-treated in T6 condition.

0022–2461

TABLE I Chemical composition of specimens

Alloy system	Specimen	Main composition (mass %)
For hardness test:		
Mg–Sc system	MS1	Sc; 1.24
	MS2	Sc; 2.84
	MS3	Sc; 6.52
Mg–Y system	MY1	Y; 2.48
	MY2	Y; 6.68
	MY3	Y; 9.34
Mg–Ho system	MH	Ho; 14.3
For tensile test:		
Mg–Y system	TMY1	Y; 0.94
	TMY2	Y; 5.34
	TMY3	Y; 8.78 (also for hardness test)
Mg–Y–Nd system	TMYN1	Y; 7.91, Nd; 2.72
	TMYN2	Y; 10.6, Nd; 2.15
Mg–Y–RE system	TMYR	Y; 10.5, RE; 2.11

2.3. Microstructure observation

Optical and scanning electron microscope (SEM) observations were performed on the specimens polished and lightly etched with 5% nitric acid, taking electron channelling patterns by the scanning electron microscope on the (0 0 0 1) plane in some specimens.

2.4. X-ray diffraction analysis

Identification of hydrides in some specimens was made by taking XRD patterns of the specimens and by referring to JCPDS (Joint Committee on Powder Diffraction Standards) cards and reported data [3–5].

2.5. Micro-Vickers hardness (MHV) test

The hardness test on the specimens before and after hydrogenation was made under a load of 1.961 N at room temperature.

2.6. Tensile test

Tensile tests were carried out on unhydrided and hydrided specimens at room temperature and up to 723 K, at a strain rate of $5.6 \times 10^{-4}\,s^{-1}$ under normal atmosphere.

3. Experimental results

3.1. Microstructure and X-ray diffraction

Optical micrographs of as cast and hydrogenated Mg–Sc, Mg–Y and Mg–Ho alloys are illustrated in Figs 1 to 3, and scanning electron micrographs of the hydrogenated alloys are in Figs 4 to 6. The figures show that flake-like ScH_2, YH_2 and HoH_2 particles have precipitated and finely dispersed in the matrix and at grain boundaries, as well as twin boundaries (see Fig. 4(c)), in the alloys, respectively; this has occurred by internal hydriding, which has been identified by XRD patterns, as illustrated in Fig. 7, referring to reported data for ScH_2 [11], YH_2 [12] and HoH_2 [13]. The dispersion mode of the hydride phases, however, is somewhat different among the alloys,

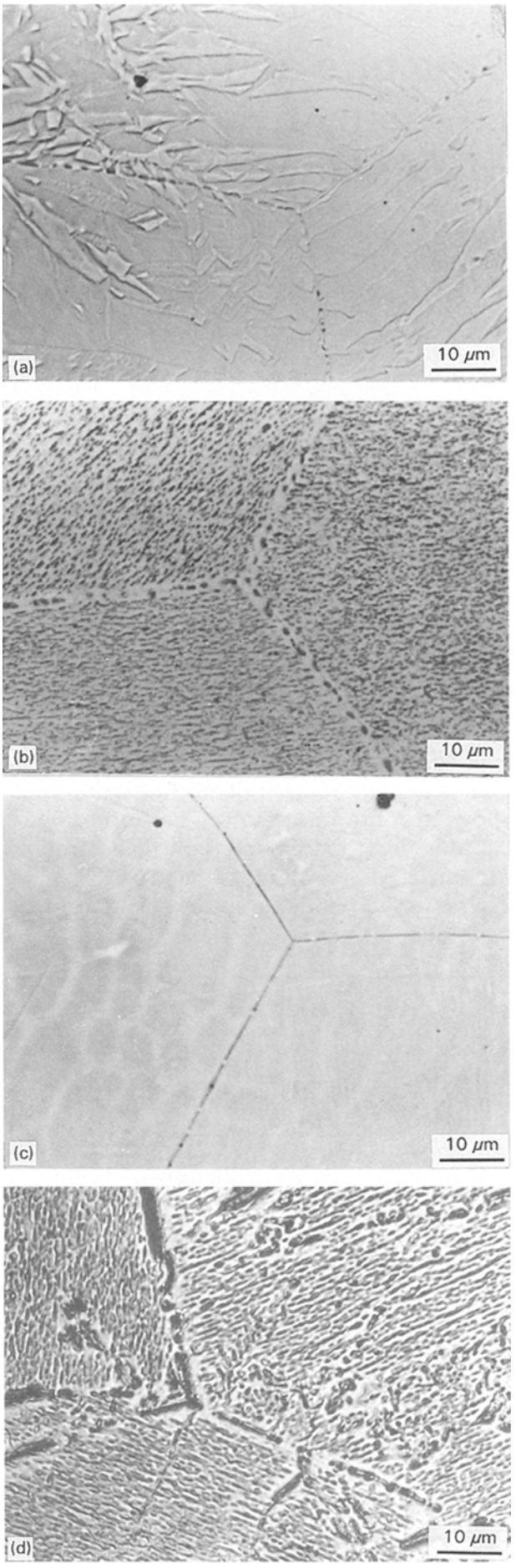

Figure 1 Optical micrographs of internally hydrided and unhydrided Mg–Sc alloys: (a) unhydrided MS1 (Mg–1.24Sc); (b) hydrided MS1; (c) unhydrided MS2 (Mg–2.84Sc); (d) hydrided MS2; (e) unhydrided MS3 (Mg–6.52Sc); (f) hydrided MS3.

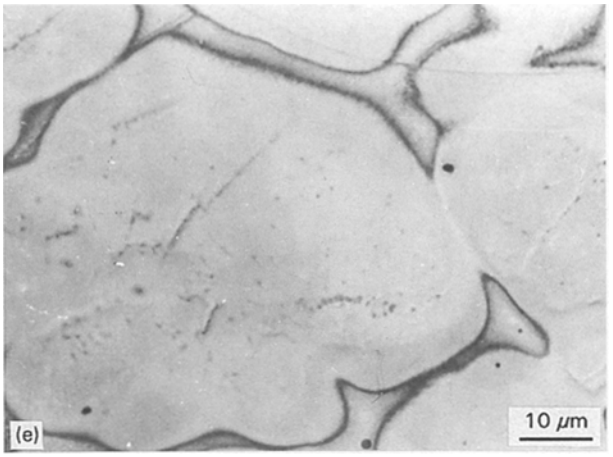

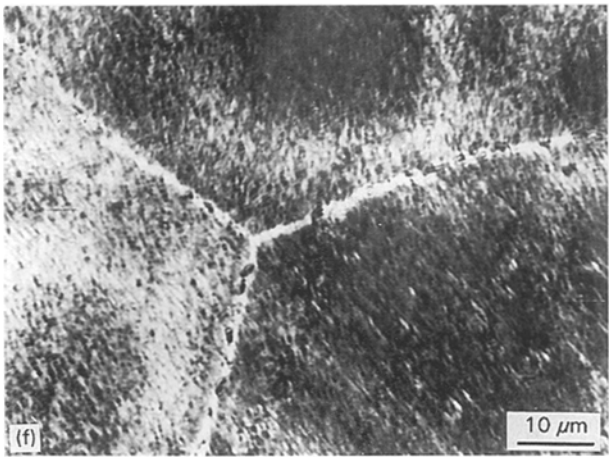

Figure 1 (continued)

which will be discussed later. The microstructure of internally hydrided Mg–Ho alloy is similar in aspect to that of Mg–Y alloys.

3.2. MHV

Change in microhardness by the hydrogenation is shown in Table II for Mg–Sc, Mg–Y, and Mg–Ho alloys. Generally, the hardness of each alloy increases with the amount of alloying element in both unhydrided and hydrided states. The hardness of internally hydrided Mg–Sc alloy, however, is higher than that of unhydrided alloy with the same Sc content, while in both Mg–Y and Mg–Ho alloys the hardness of hydrided alloys is lower than that of unhydrided alloys. This discrepancy in change of hardness by internal hydriding between the former alloy and the latter two may be attributed to the difference in solution-hardenability of the alloying elements, Sc, Y and Ho. This fact will be discussed later.

3.3. Tensile properties

Short-time tensile properties of the hydrided TMY1 (Mg–0.94Y), TMY2 (Mg–5.34Y) and TMY3 (Mg–8.78Y) are shown in Fig. 8. Even though the strength of hydrided alloys is lower than that of unhydrided alloys up to 673 K, as illustrated in Table III for TMY3, above 673 K the strength of hydrided alloys containing more than approximately 2 mass %

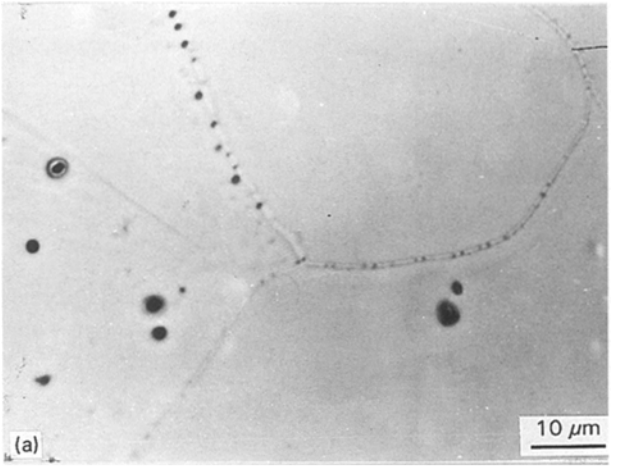

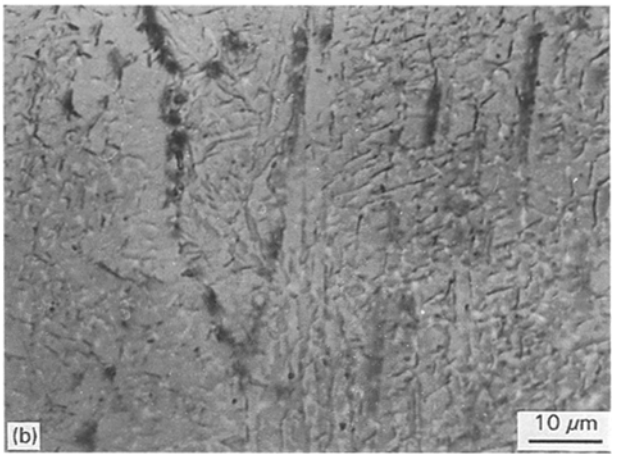

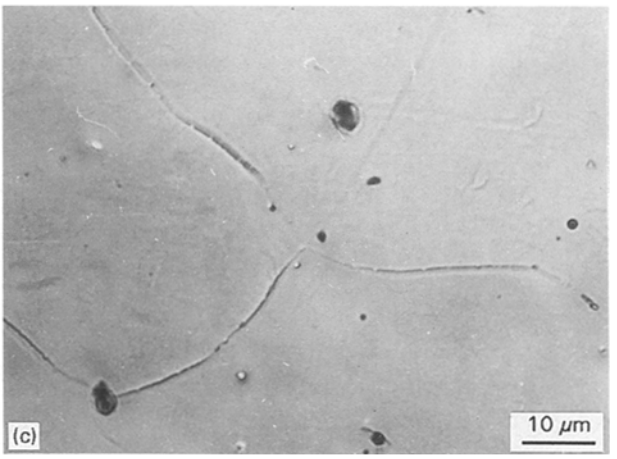

Figure 2 Optical micrographs of internally hydrided and unhydrided Mg–Y alloys: (a) unhydrided MY1 (Mg–2.48Y); (b) hydrided MY1; (c) unhydrided MY2 (Mg–6.68Y); (d) hydrided MY2; (e) unhydrided MY3 (Mg–9.34Y); (f) hydrided MY3.

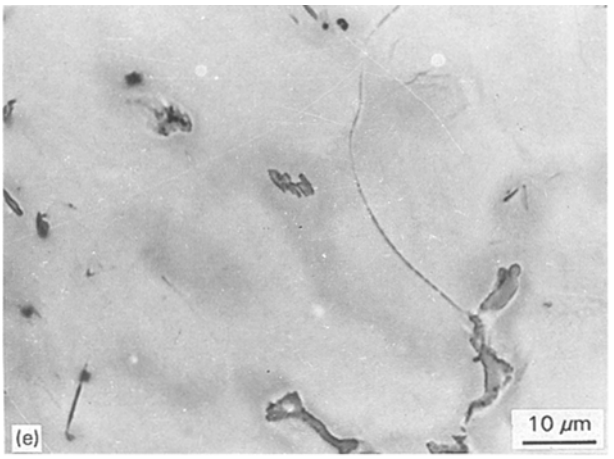

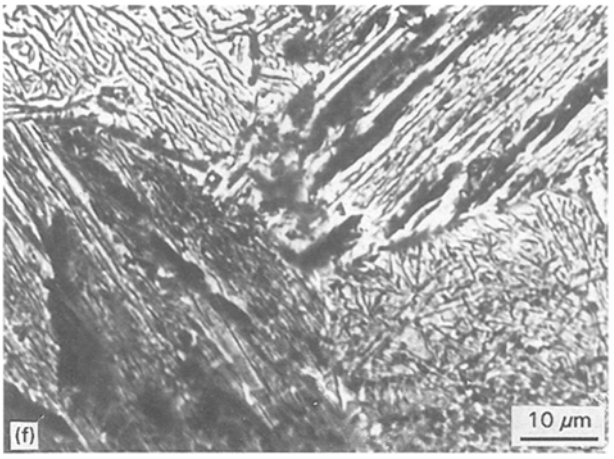

Figure 2 (continued)

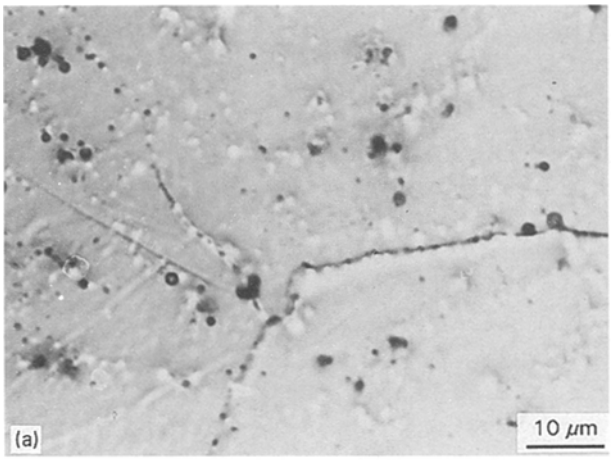

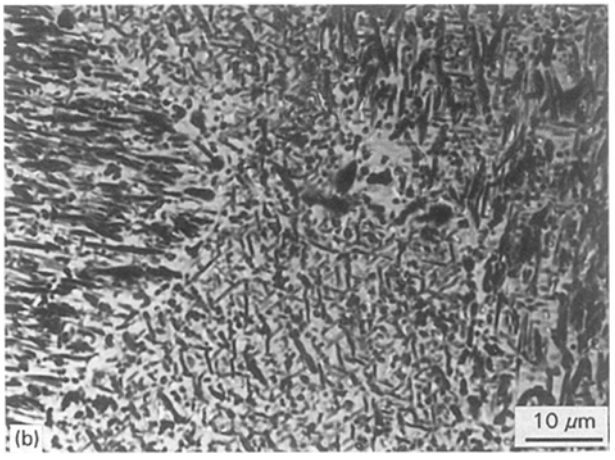

Figure 3 Optical micrographs of (a) unhydrided and (b) internally hydrided MH (Mg–14.3Ho).

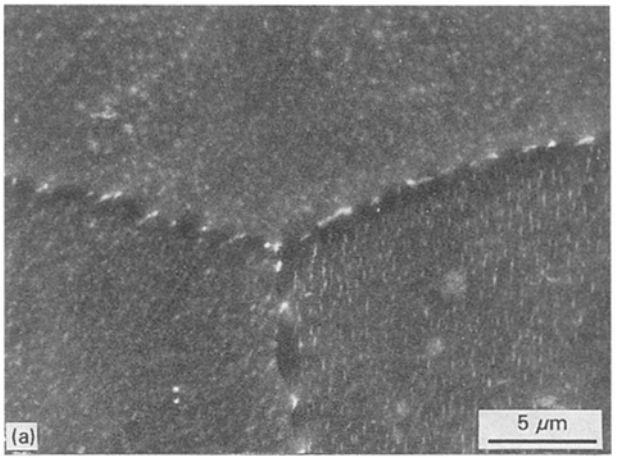

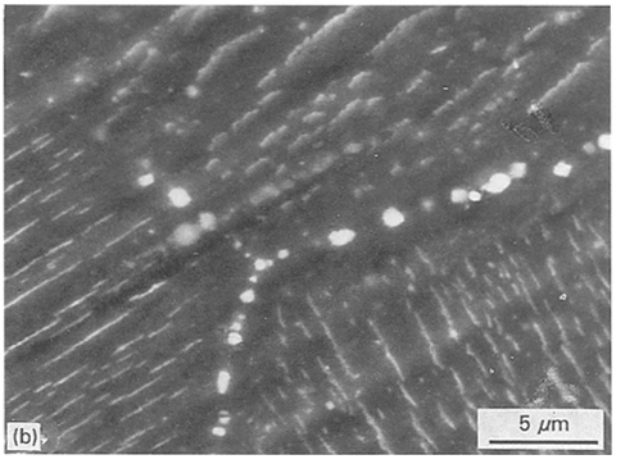

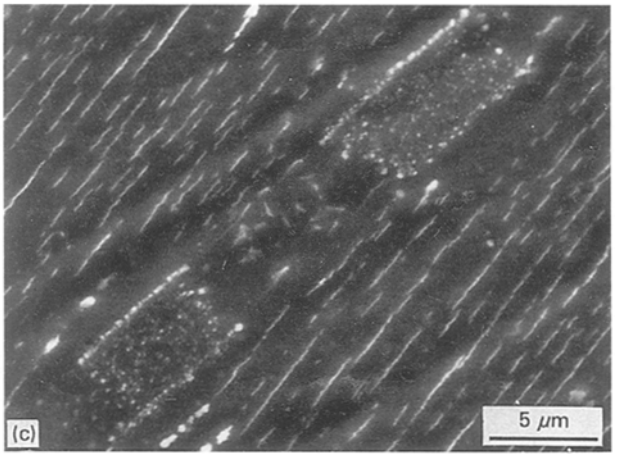

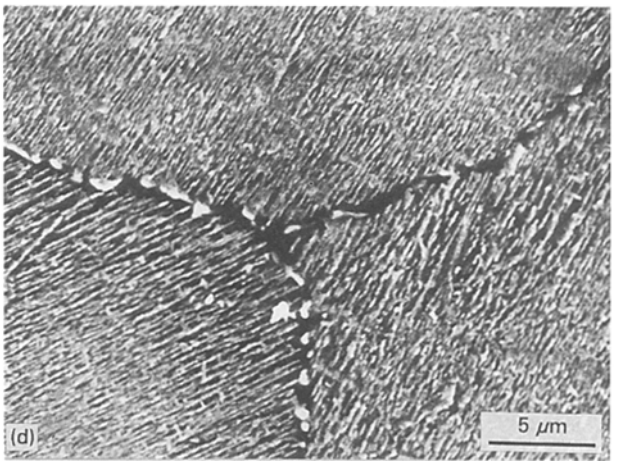

Figure 4 Scanning electron micrographs of internally hydrided Mg–Sc alloys: (a) MS1 (Mg–1.24Sc); (b) MS2 (Mg–2.84Sc); (c) MS2 with precipitates at twin boundaries; (d) MS3 (Mg–6.52Sc).

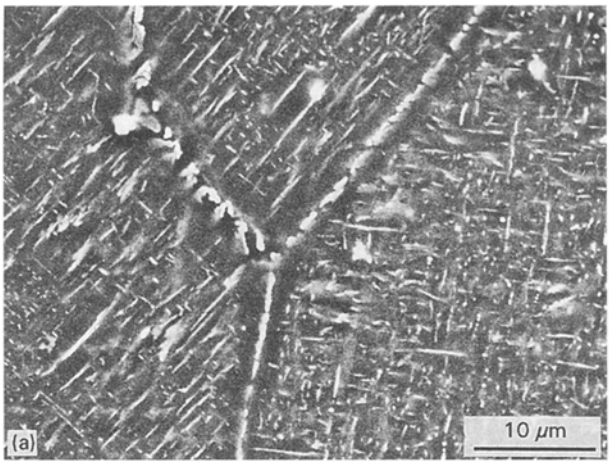

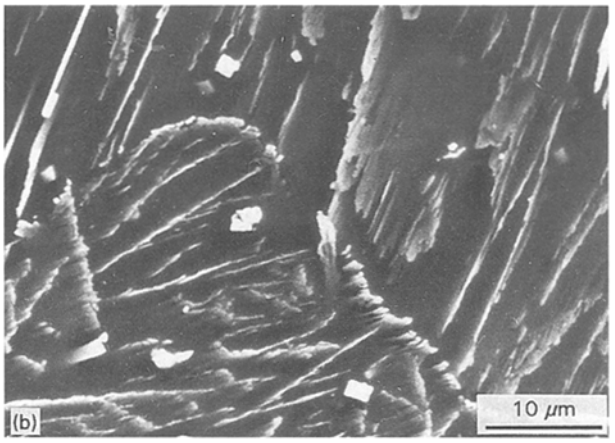

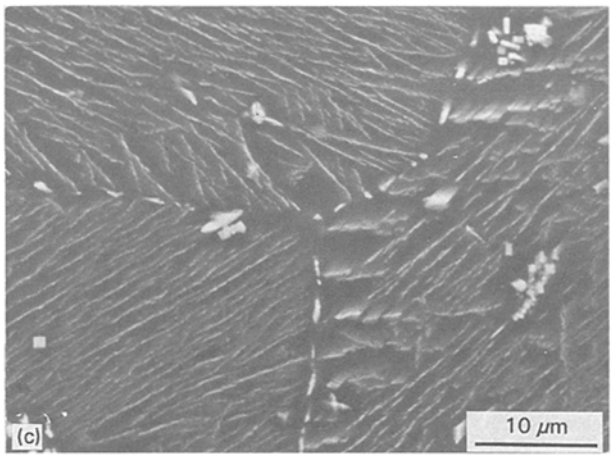

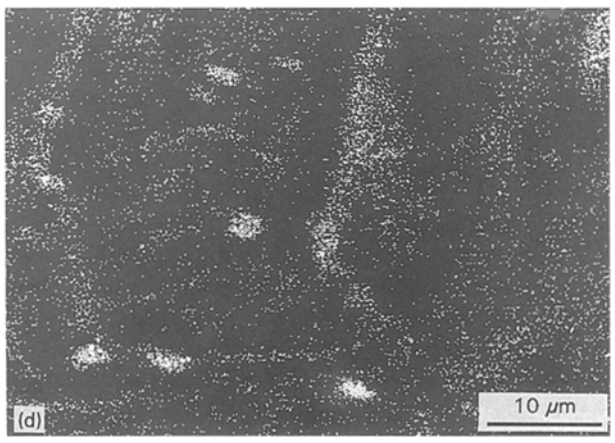

Figure 5 (a–c) Scanning electron micrographs and (d) Y–K_α X-ray image of internally hydrided Mg–Y alloys: (a) MY1 (Mg–2.48Y); (b) and (d) MY2 (Mg–6.68Y); (c) MY3 (Mg–9.34Y).

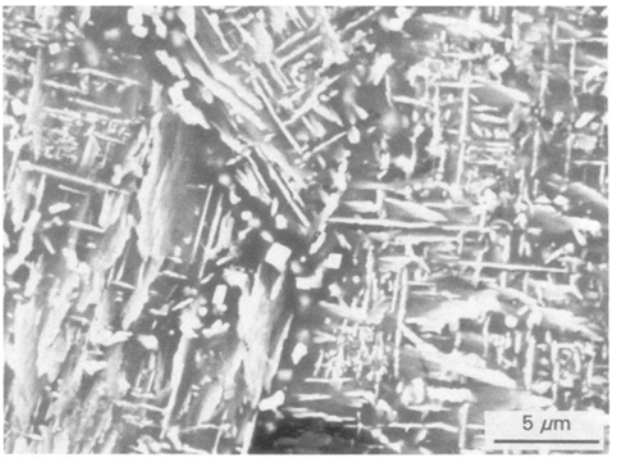

Figure 6 Scanning electron micrograph of internally hydrided MH (Mg–14.3Ho).

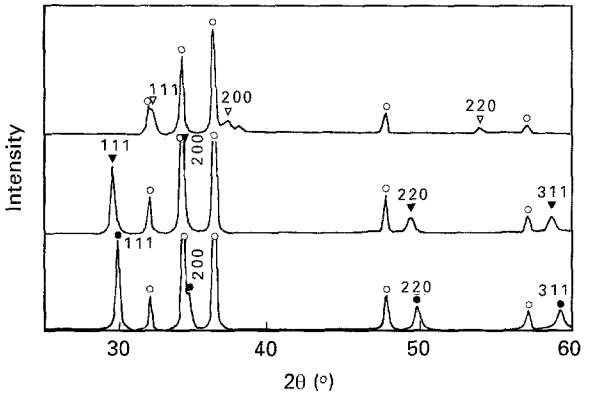

Figure 7 X-ray diffraction patterns for internally hydrided MS1 (Mg–1.24Sc), MY1 (Mg–2.48Y) and MH (Mg–14.3Ho) alloys. ○ Mg; ▽ ScH_2; ▼ YH_2; ● HoH_2.

TABLE II Micro-Vickers hardness (MHV) of specimens before and after hydrogenation

Specimen	Before	After
MS 1	32.5	42.6
MS 2	32.1	42.7
MS 3	51.3	70.0
MY 1	45.1	38.8
MY 2	71.2	49.3
MY 3	76.8	57.7
MH	70.7	58.5
TMY3-1 (Fully hydrogenated[a])	77.0	58.5
TMY3-2 (1/2 hydrogenated[a])	77.0	68.4
TMY3-3 (1/3 hydrogenated[a])	77.0	63.8

[a] See the text.

of yttrium is expected to be almost the same or higher than that of unhydrided alloys with the same amount of yttrium. Above 573 K unhydrided alloys are superior in elongation to hydrided alloys.

Table III also shows tensile properties of TMYR (Mg–10.5Y–2.11RE) and TMYN2 (Mg–10.6Y–2.15Nd) before and after hydrogenation, which implies that the tensile strength of hydrided alloys at 673 K is higher than that of unhydrided alloys, while elongation of hydrided alloys is less than that of unhydrided ones.

Table IV illustrates the change in tensile properties at 723 K of TMY3 (Mg–8.78Y) by the treatment at various degrees of hydrogenation. Microscopic examination of the treated specimens showed that the TMY3-2 specimen had the finest distribution of hydrides among three hydrogenated specimens in the table. This fact may imply that an optimum period of hydrogenation exists, and a longer period of hydrogenation induces the growth of hydride particles and depletion of solute in the matrix, both of which result in the lowering of high-temperature strength of internally hydrided specimens.

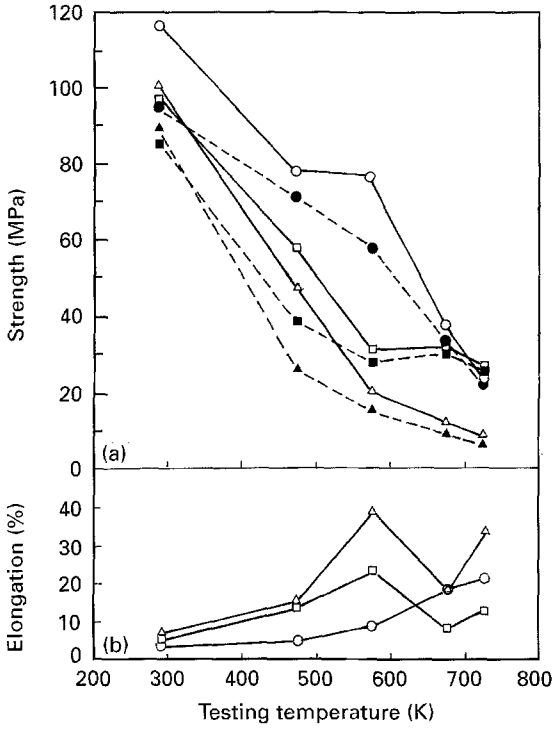

Figure 8 Yttrium content dependence of short-time tensile properties of internally hydrided Mg–Y alloys: TMY1 (Mg–0.94Y); TMY2 (Mg–5.34Y); TMY3 (Mg–8.78Y). Triangles TMY1, squares TMY2, circles TMY3. (a) Strength, open symbols UTS, closed symbols YS. (b) Elongation.

4. Discussion

As mentioned above, although finely dispersed hydride precipitates were formed in the matrix of internally hydrided Mg–III_a transition metal alloys, the hardness and tensile properties at room temperature were degraded in the Mg–Y and Mg–Ho alloys, while the hardness of Mg–Sc alloys was improved by the hydriding. This discrepancy may be explained by the different degrees of solution hardenability of added elements and/or different aspects of precipitation behaviour of hydrides.

The atomic size of Mg, Sc, Y, and Ho is 0.320, 0.330, 0.364 and 0.350 nm, respectively. Since addition of Y and/or Ho to magnesium can solution-harden the matrix more strongly than does Sc, then the softening of the matrix itself by the depletion of solute due to the precipitation of hydride may be larger in Mg–Y and Mg–Ho alloys than in Mg–Sc alloy. On the other hand, the hardening by the precipitation may depend on various factors, such as size, interspacing and distribution mode of precipitate particles. Then, the resulting strength of internally hydrided alloys may be attributed to the combination of the two hardening mechanisms: the solution hardening by remaining solute elements and the dispersion hardening due to the formation of hydride precipitates.

As shown in Figs 1 to 6, hydride precipitates in the alloys seem to have some crystallographic orientation relationship to the matrix, from which they have come. At a glance, the figures suggest that three main equivalent crystallographic planes of precipitation exist in the matrix for Mg–Y and Mg–Ho alloys, while only one plane exists for Mg–Sc alloy. Further observations with electron channelling patterns and SEM micrographs taken in the basal plane of the matrix show (referred to in a review [14]) that ScH_2 platelets have mainly formed on the basal plane of Mg lattice with preferential growth directions, probably $\langle 1\,1\,2\,0 \rangle_{Mg}$, in the Mg–Sc alloy (as shown in Fig. 9) while plate-like YH_2 aggregates have aligned approximately along prismatic planes of Mg lattice in the Mg–Y alloy (as shown in Fig. 10) the surface of which is also parallel to the basal plane. Then, the aggregates

TABLE III Tensile properties of TMYN2 (Mg–10.6Y–2.15Nd), TMYR (Mg–10.5Y–2.11RE) and TMYN1 (Mg–7.91Y–2.72Nd) alloys before and after hydrogenation, with TMY3 (Mg–8.78Y) alloy as a reference

Test temperature	RT			523 K			673 K		
Tensile property	UTS (MPa)	YS (MPa)	E (%)	UTS (MPa)	YS (MPa)	E (%)	UTS (MPa)	YS (MPa)	E (%)
Specimen:									
Unhydrided TMYN2	197	180	1.2	–	–	–	38	38	15.8
Hydrided TMYN2	192	140	4.5	82	71	12.0	50	43	5.0
Unhydrided TMYR	–	–	–	–	–	–	37	34	161.8
Hydrided TMYR	134	116	0.4	–	–	–	53	43	6.6
Unhydrided TMYN1	194	178	1.0	–	–	–	–	–	–
Hydrided TMYN1	189	138	4.5	80 (573K)	70	11.9	–	–	–
Unhydrided TMY3[a]	191	164	3.0	155	113	12.3	46	39	29.0
Hydrided TMY3	117	95	4.0	75	57	9.8	37	34	18.0

– Not tested.
[a] T6 condition.

TABLE IV Tensile properties at 723 K of TMY3 (Mg–8.78Y) alloys treated in various conditions

Specimen	Condition	UTS (MPa)	YS (MPa)	E (%)
TMY3-1	Fully hydrogenated[a]	24.1	22.0	21.3
TMY3-2	1/2 hydrogenated[a]	37.2	34.2	25.8
TMY3-3	1/3 hydrogenated[a]	31.2	29.7	28.0
Unhydrided TMY3	T6 heat-treated	24.1	23.1	93.5

[a] See the text.

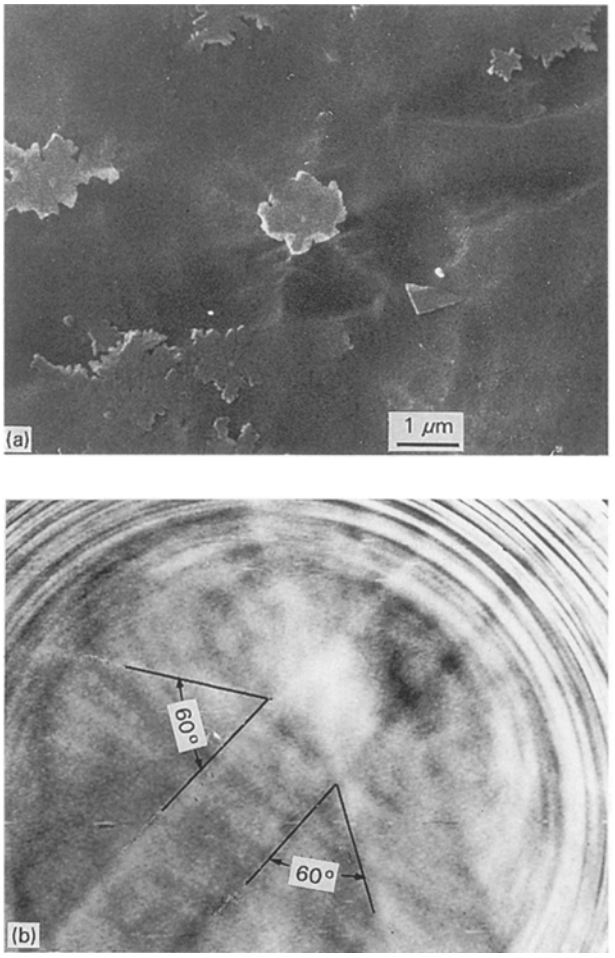

Figure 9 (a) Scanning electron micrograph and (b) electron channelling pattern on near (0 0 0 1) plane of MS1 (Mg–1.24Sc).

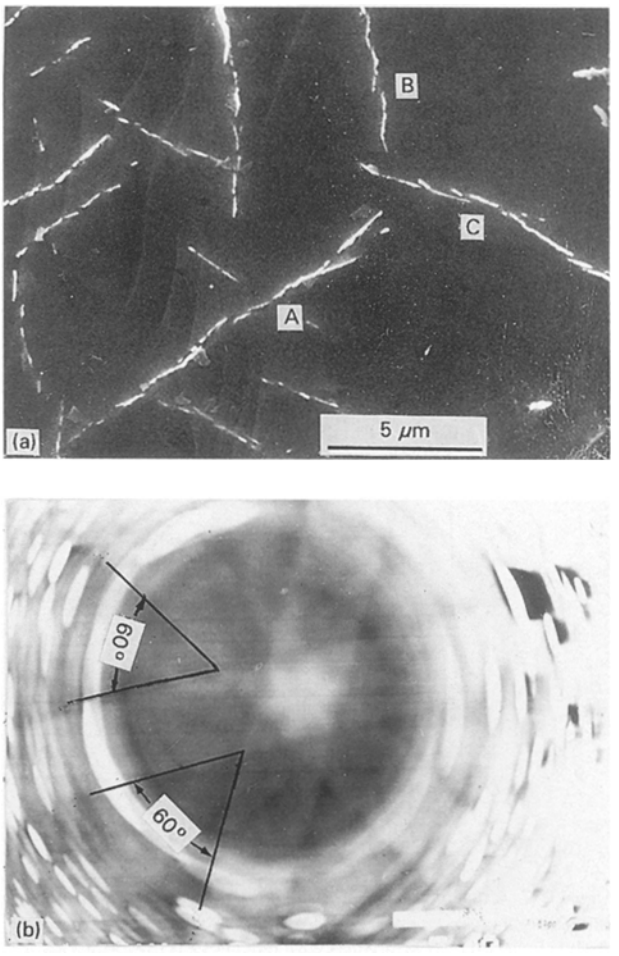

Figure 10 (a) Scanning electron micrograph and (b) electron channelling pattern on near (0 0 0 1) plane of MY1 (Mg–2.48Y).

with three different growth directions make an angle of 60 or 120° with each other, for example A, B and C in Fig. 10. With the figures, the main coincidence between hydrides and the matrix is presumed to be $(0\,0\,0\,1)_{Mg}//\{1\,1\,1\}_{ScH_2}$ in the Mg–Sc alloy and $\{1\,1\,2\,0\}_{Mg}//\{1\,0\,0\}_{YH_2}$ in the Mg–Y alloy, as drawn in Fig. 11. In the case of Mg–Y alloy (Fig. 10), however, each aggregate has taken a branching (e.g. A, B or C in Fig. 10). By further investigation, two groups of branching angle have been observed: one is 16–19° (e.g. C in Fig. 10) and the other is 22–27° (e.g. A and B in Fig. 10). Then, these groups of angle are presumed to be deviations from main coherent interface of $\{1\,1\,2\,0\}_{Mg}$ and $\{1\,0\,0\}_{YH_2}$ to the interface of $\{1\,3\,4\,0\}_{Mg}$ and $\{4\,1\,0\}_{YH_2}$ for the former branching, and to the interface of $\{1\,4\,5\,0\}_{Mg}$ and $\{3\,1\,0\}_{YH_2}$ for the latter branching. This is because the angle between $\{1\,1\,2\,0\}_{Mg}$ and $\{1\,3\,4\,0\}_{Mg}$ is calculated as 16° geometrically, and the angle between $\{1\,0\,0\}_{YH_2}$ and $\{4\,1\,0\}_{YH_2}$ is 15°, while the angle between $\{1\,4\,5\,0\}_{Mg}$ and $\{1\,1\,2\,0\}_{Mg}$ is 20°, and the angle between $\{1\,0\,0\}_{YH_2}$ and $\{3\,1\,0\}_{YH_2}$ is 19.5°, even though some discrepancies between observation and calculation are present. This branching mentioned above may occur in order to minimize interfacial stress between hydrides and the matrix. Even though short-time tensile properties at room temperature of internally hydrided Mg–Y alloy are inferior to those of unhydrided alloy, the high-temperature strength of hydrided alloy is comparable or superior to that of unhydrided alloy. For instance, as shown in Fig. 12, load versus elongation curves of hydrided and unhydrided Mg–10.6Y–2.15Nd alloys tested at 673 K illustrate different deformation behaviours: strain hardening can be seen in the curve of hydrided specimen, while softening occurs immediately after yielding in the unhydrided specimen.

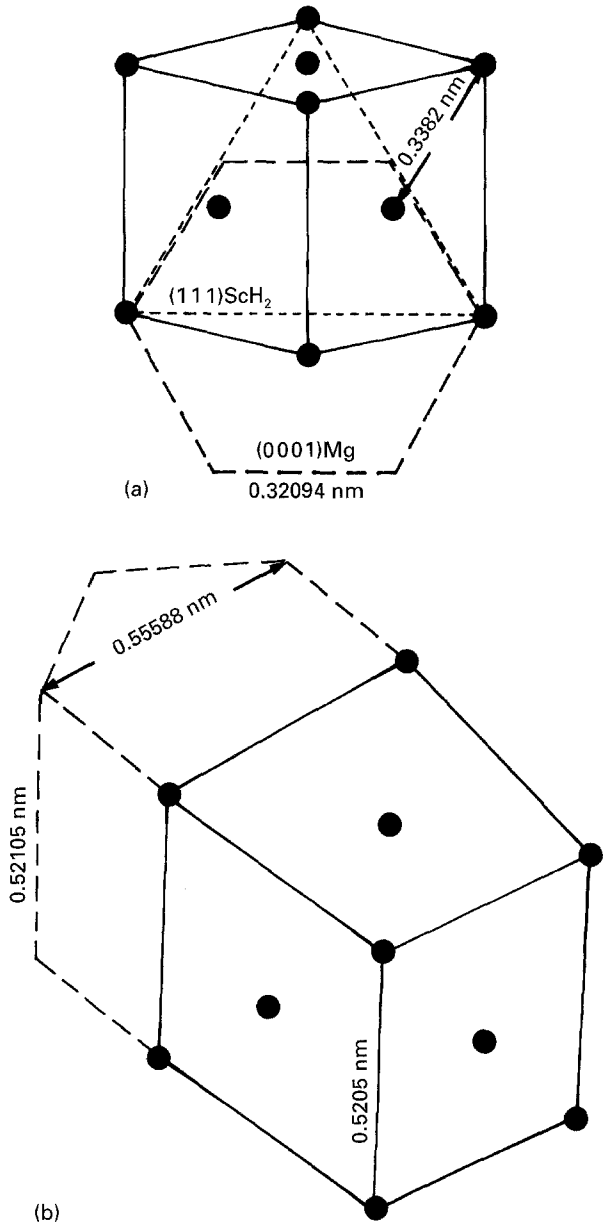

Figure 11 Presumed schemes of crystallographic coincidence between magnesium and hydrides: (a) Mg/ScH_2 interface where $(0\,0\,0\,1)_{Mg}//(1\,1\,1)_{ScH_2}$; solid lines with filled circlets (Sc atoms) are for ScH_2 lattice, dotted lines are for $(1\,1\,1)_{ScH_2}$, and broken lines are for the basal plane of Mg lattice. (b) Mg/YH_2 interface where $(1\,1\,2\,0)_{Mg}//(1\,0\,0)_{YH_2}$; solid lines with filled circlets (Y atoms) are for YH_2 lattice, and broken lines are for Mg lattice.

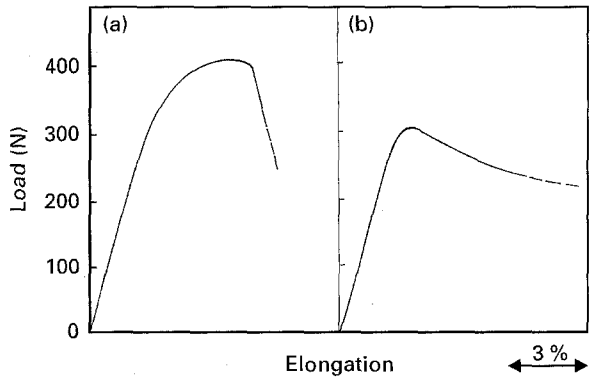

Figure 12 Load versus elongation curves at 673 K of (a) internally hydrided and (b) unhydrided TMYN2 (Mg–10.6Y–2.15Nd).

Furthermore, the short-time tensile properties of hydrided alloy at high temperature, say 673 K, are equivalent or superior to those of Mg–Th alloys [15], and the hydride phase is very stable, at least up to 773 K. Therefore, it can be expected that the internally hydrided Mg–Y alloy may have a good creep resistance at high temperature. Meanwhile, Table III seems to imply that the minor addition of other rate earth elements, such as Nd and RE (Mischmetal), improves the tensile strength of hydrided Mg–Y alloys at room temperature, though addition of RE lowers the ductility of the alloys.

Finally, it can be noted from Table IV that when internally hydrided magnesium alloys of this kind are considered for practical use, finding the optimum hydriding conditions for creep properties may be very important.

5. Summary

In spite of lower tensile properties of internally hydrided Mg–III_a transition metal alloys than those of unhydrided alloys at room temperature and up to about 673 K, above this temperature range the internally hydrided alloys are expected to have outstanding tensile properties, especially creep resistance, due to finely dispersed hydrides both in the matrix and at the grain boundaries.

Acknowledgements

The authors are grateful to Messrs T. Ohshima and M. Hirabayashi for their assistance in the experimental work.

References

1. E.F. EMLEY, "Principles of magnesium technology" (Pergamon Press Ltd., Oxford, 1966).
2. F. SAUERWALD, *Z. Metallkunde* **40** (1949) 44.
3. J. HÉRENGUEL and J. BOGHEN, *Memo. Scien. Rev. Mét.* **56** (1959) 371.
4. H. TASCHOW and F. SAUERWALD, *Z. Metallkunde* **52** (1961) 135.
5. P. LELONG, J. DOSDAT, J. BOGHEN and J. HÉRENGUEL, *J. Nucl. Mater.* **3** (1961) 222.
6. J. HÉRENGUEL, *Ibid.* **8** (1963) 12.
7. G.T. HIGGINS and B.W. PICHLES, *Ibid.* **8** (1963) 160.
8. R.P. KENT and T.C. WELLS, *Ibid.* **8** (1963) 198.
9. E.A. WALKER and P.A. FISHER, *Ibid.* **8** (1963) 179.
10. R.L. SQUIRES, R.T. WEINER and M. PHILLIPS, *Ibid.* **8** (1963) 77.
11. J. MCGUIRE and C.P. KEMPTER, *J. Chem. Phys.* **33** (1960) 1584.
12. C.E. LUNDIN and J.P. BLACKLEDGE, *J. Electrochem. Soc.* **109** (1962) 838.
13. A. PEBLER and W.E. WALLACE, *J. Phys. Chem.* **66** (1962) 148.
14. D.C. JOY, D.E. NEWBURY and D.L. DAVIDSON, *J. Appl. Phys.* **53** (1982) R81.
15. R.S. BUSK, "Magnesium products design" (Marcel Dekker, Inc., New York, 1987).

Received 4 November 1994
and accepted 13 February 1996